# Embedded acoustic sensing and monitoring techniques for small modular reactors

L.B. Beardslee, R. Schoenemann, M. Remillieux, G. Rodriguez, B. Maiorov, M. Jaime, and T.J. Ulrich.

## 1 Introduction

The goal of this project was to study the applicability of specific innovative instrumentation techniques for assessing parameters needed for safe small modular reactor operation and safeguarding of nuclear material.  Small modular reactor core designs are currently being developed to provide energy more effectively and efficiently than in the past because they can be built as modules at fabrication sites and then transported to a power-producing facility.  However, these modules and/or the final core will often be sealed and not accessible again until disposal. Instead of instruments that access the core directly, during and after operation, to monitor flux/dose and structural integrity, as current power plants use, new sensors need to be designed that can be built into the reactor initially to determine operating history, structural integrity through operation of the system, and nuclear material accountancy after shutdown and before disposition of the core.  Embedded sensors already exist that can provide neutron flux, gamma dose, and temperatures, but techniques to expand upon these for assessing structural health and material inventory in the system over time need to be developed. Structural health assessments include the detection and imaging of cracks in the components that could eventually cause radioactive fission products to be released.

In this project, we investigated two innovative technologies, more specifically, 1) Resonant Ultrasound Spectroscopy (RUS) for material characterization and its nonlinear variant (NRUS) for general damage detection and one sensing technology: fiber Bragg gratings (FBG) in optical fibers.

## 2 Scientific Approach and Results

### 2.1 Resonant Ultrasound Spectroscopy

Resonant ultrasound spectroscopy (RUS) is a powerful non-destructive technique used to measure the full elastic tensor (elastic constants), as well as other information such as density, anisotropy and texture, of a material based on the resonance frequencies of vibration of an object. [1] The original formulation of this technique has restrained its application to careful laboratory study and relatively simple situations in which the sample has a trivial geometry (e.g., block, cylinder, sphere) and is vibrated in a specific manner. Considerable efforts have recently been devoted by our team to making this technology applicable to the field, by extending it to complex sample geometries, multi-material systems, and non-standard sources of vibration. In the context of small modular reactor operation, RUS should take advantage of the ambient sources of vibration to measure the resonance frequencies of the system.

Traditionally, the sample would be excited with a sequence of sinusoidal signals sweeping a pre-determined frequency range. This process allows for high signal:noise ratios and a precise means of obtaining the natural vibrational frequencies necessary for a RUS inversion, however, requires placement, contact, and control of an acoustic/ultrasonic source or actuator. Use of a physical actuator is not desirable for *in situ* application, especially in the present context of nuclear reactors. Alternatively, here the feasibility of using ambient noise excitations as an alternative methodology for RUS measurement was explored and achieved in the laboratory. The sample under test was a reactor core-block made by additive manufacturing, as shown in Fig. 1. This sample was in contact with a piezoelectric transducer that was driven for 20s with band-limited white noise, i.e., a random excitation signal in the range of 1-20 kHz. The use of a physical transducer was necessary here for reproducibility; however, environmental noise would be used in practice. The time series and spectrum for the white noise used for this experiment are shown in Fig. 2.



Figure 1: Experimental setup for evaluating the feasibility of using ambient noise for RUS measurements.
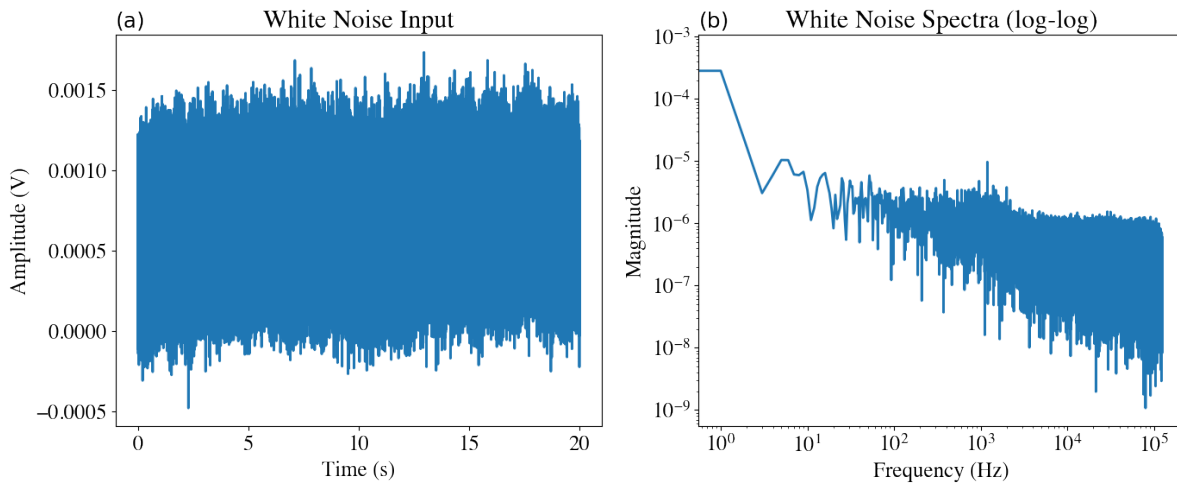


Figure 2: White-noise signal used to drive the piezoelectric transducer: (a) waveform and (b) spectrum

2

The vibrational response on the sample was measured without contact using a laser vibrometer. In the field, the vibrational response would be measured by embedded fiber-optic sensors or other dynamic strain sensors. The waveform of the vibrational signal measured with the laser is shown in Fig. 3a. Initially, we used the fast Fourier transform (FFT) of the waveform to calculate its spectrum, as shown in Fig. 3b. Some resonance frequencies may be identified but the noise level is very high. As an alternative to taking the FFT of the complete signal, the original signal was separated into 100ms adjacent time windows. Each of these windows are auto-correlated to obtain the local empirical Green functions, from which the spectra can be obtained. The resulting spectra from each window are averaged to obtain a high signal-to-noise ratio spectrum of the resonant modes (see Fig. 3c – red spectrum). Other alternative methods, e.g., Welch's method, wavelet transforms, etc., may also provide equivalent signal to noise improvements over a single FFT of the complete signal. This will be explored in future studies, however, the auto-correlation method used here proved sufficient to extract precise modal information necessary for the selected resonance techniques. The modal frequencies obtained in this manner from white-noise response also show good agreement with those from standard stepped-sine methods, Fig. 3c – blue curve, though, the white-noise methodology does not appear to capture all of the modes present.
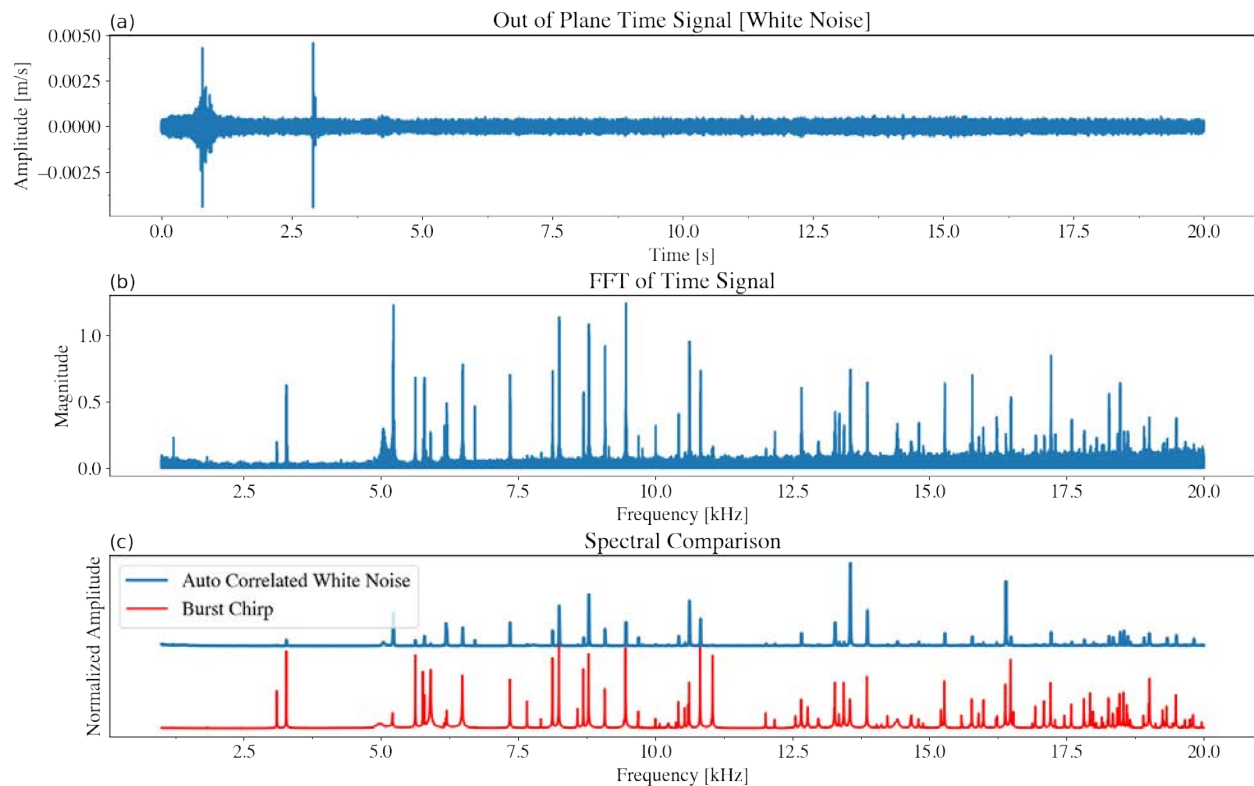


Figure 3: Vibrational response of the sample excited with white noise: (a) waveform, (b) FFT with no pre-processing, (c) FFT with auto-correlation pre-processing.

From this simple experiment and with the appropriate signal processing technique in place, ambient vibration may be used successfully to measure the resonance spectrum of an object in-situ. Such information may in turn be used to track changes in the system, which could include a crack, change of stiffness, change of mass, etc.

The next set of experiments we conducted aimed at evaluating the ability of RUS to detect small changes in a system. For this experiment, we used a smaller sample manufactured by additive manufacturing, as

shown in Fig. 4. In one of the experiments, the original sample was vibrated while the vibrational response was recorded with a laser vibrometer. In another experiment, a small mass was glued to the sample. In a third experiment, we used a similar sample that was cut in half and welded back into one piece. The experiments were conducted using traditional excitation signals and white noise. In all cases, RUS could detect a change with results summarized in Fig. 5.



Figure 4: Experimental setup used to demonstrate the ability of RUS to detect small changes in a system.
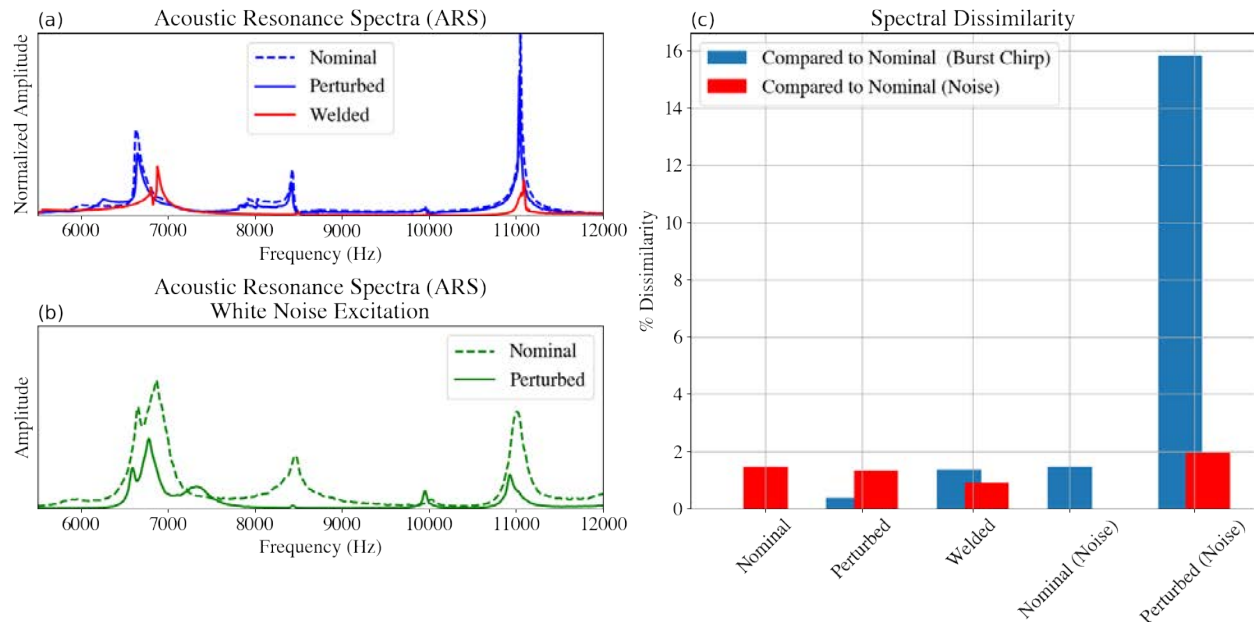


Figure 5: Result of the sensitivity experiments using RUS: (a) comparison of original sample, perturbed (added mass) sample, and cut/welded sample using traditional excitation, (b) comparison of original and perturbed sample with white-noise excitation, (c) summary.

The last step of RUS processing involves using the resonance frequencies of the system to solve an inverse problem to find elastic properties of the system. For this step to be successful, a set of vibrational mode shapes simulated with an approximate set of elastic properties should match the measured ones. An example of such task on the larger sample is shown in Fig. 6. The match between predicted and measured vibrational mode shapes is excellent. Such measurements could possibly be done in situ with embedded sensors if the sensors are distributed throughout the sample (e.g., fiber optics) and their positions were precisely known.
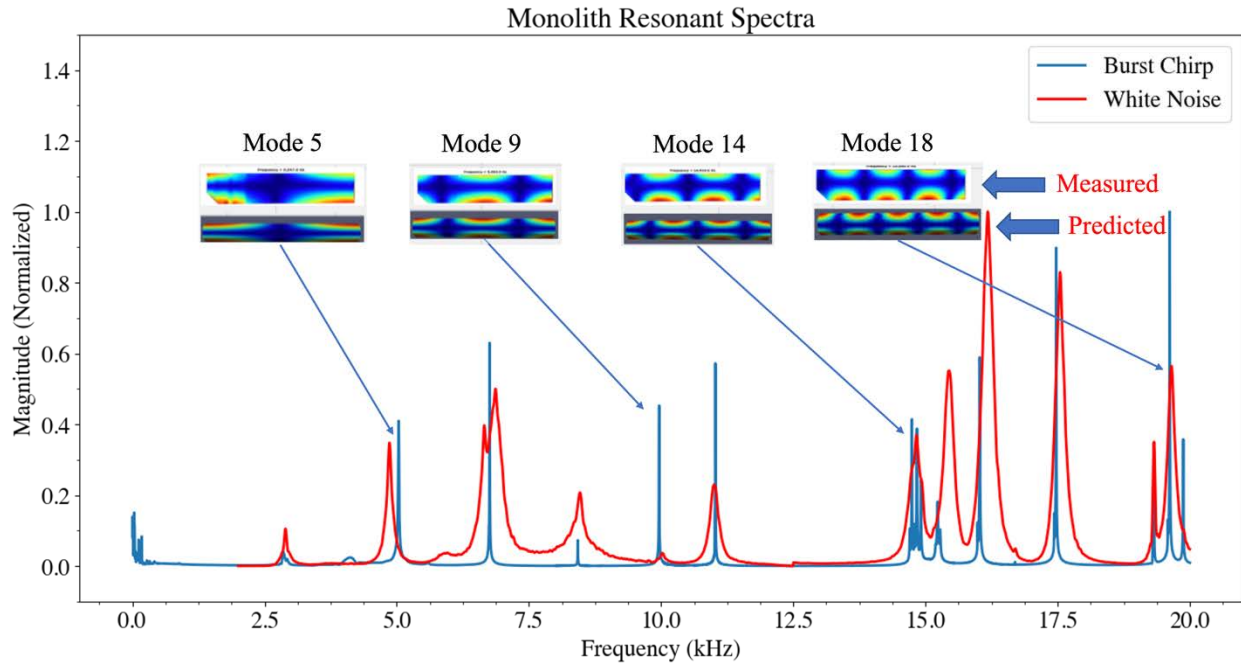
Figure 6: Resonance spectrum and mode shapes (both predicted and measured) for the large sample shown in Fig. 4.

## 2.2 Nonlinear Resonant Ultrasound Spectroscopy

The next step of the resonance detection tool is based on the nonlinear version of RUS. NRUS extends traditional RUS to exploit the nonlinear behavior of damaged materials to increase sensitivity to certain types of damage which can be quantified from the amplitude dependence of the engineering moduli or the resonance frequencies. [2] Instead of focusing on the full resonance spectrum, NRUS is usually focused on one resonance frequency and its possible dependence on vibrational amplitude if the sample contains some nonlinear features, such as cracks, delaminations, disbonds, etc.

A sample with a representative crack or flaw was unable to be obtained for this initial study. To bypass the lack of a cracked sample, we considered a rod of Berea sandstone, which is a known nonlinear material due to a complex mesoscopic structure with internal microcracks and pore structure and compared its NRUS response to that of an acrylic sample when using white-noise excitation. Results are shown in Fig. 7. The resonance frequencies of the sandstone are clearly amplitude dependent, which is evidence of a nonlinear behavior, whereas the acrylic has a perfectly linear response, i.e., no change as a function of the vibrational strain amplitude. This simple experiment shows the potential of ambient noise to be used for NRUS testing.
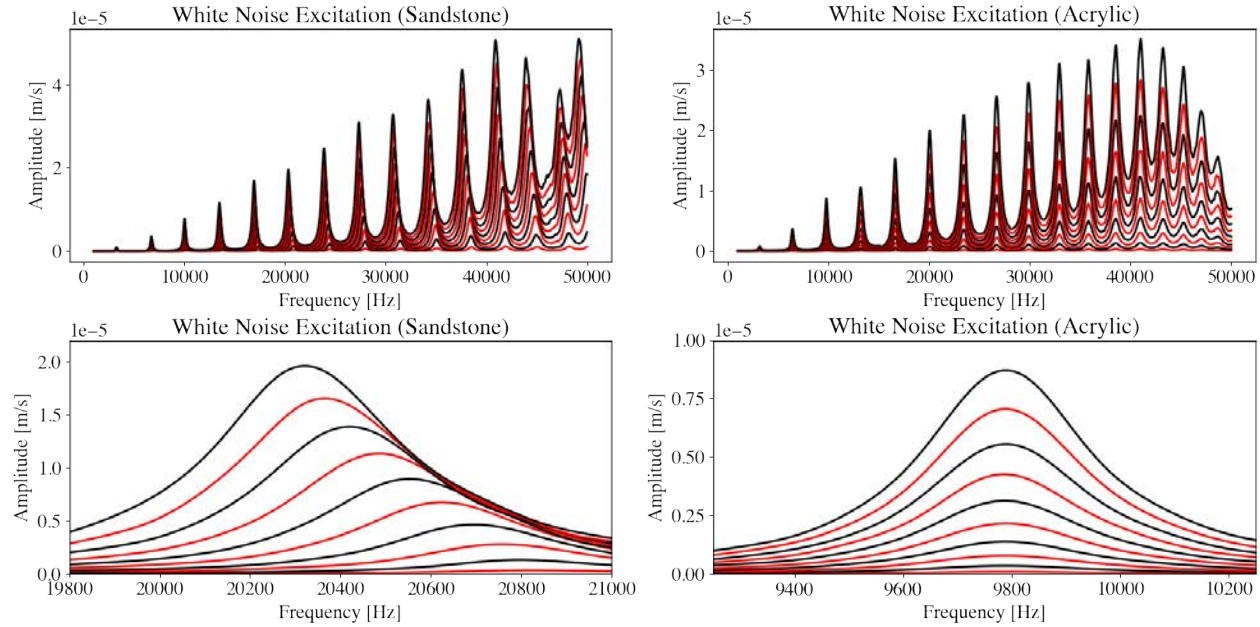
Figure 7: NRUS results obtained with white noise on a sample of Berea sandstone (left) and acrylic (right).


## 2.3   Fiber Optic Sensing

Sensors based on Fiber Bragg Gratings (FBG's) are promising candidates for embedded sensing and structural health monitoring applications due to their small size, high sensitivity, multiplexing capabilities and their robustness to electromagnetic noise, radiation, and extreme temperatures. Their development in the field of structural health monitoring was pioneered by Satori *et al.* [3] and has since attracted significant interest (see for instance refs. [4-6] for reviews of state of the art techniques).

In this section we explore the capabilities of an FBG interrogation technique, currently in use at MPA-MAGLAB, as part of an embedded sensing project for potential applications in structural failure detection in microreactors. We present a brief description of our technique and demonstrate its capabilities to detect mechanical resonances and acoustic emission signals as well its tolerance to radiation exposure.

The FBG interrogation technique utilized in this project is currently in use at MPA-MAGLAB and is designed for low temperature strain measurements in pulsed magnetic fields [7] to study the magnetostriction of mm sized samples. Unlike common demodulation techniques that interrogate the FBG reflection or transmission spectrum at a single wavelength located at the linear flank of the peak and translate the change of amplitude into strain, our method records the entire FBG spectrum in a wide wavelength range of about 50 nm centered around 1550 nm. Depending on the width of the reflection peak, this technique allows for a simultaneous detection of up to $\approx$ 50 gratings that can be distributed over a desired length of a single optical fiber.

A schematic drawing of the setup is displayed in Fig. 8a. Light from a broadband superluminescent diode (SLD) source (Thorlabs, Fiber-coupled SLD Source) is coupled into a single mode optical fiber, which passes an optical attenuator and circulator before it reaches the FBG. The reflected light enters a spectrometer (Princeton Instruments, Acton SP2500) equipped with a 600 nm diffraction grating and is detected with a 1024-pixel InGaAs digital linescan camera (SUI, SU1024-LDH-1.7RT-0500/LC) with a

6

maximum line rate of 46992 Hz. A typical reflection peak of a single FBG is shown in Fig. 8b.  The strain resolution of this setup is mostly limited by the readout noise of the InGaAs detector and can reach up to 0.1 με at 46992 Hz.

In this work we used commercially available polyimide and ormorcer coated and $GeO_2$ doped single mode optical fibers with a diameter of 125 μm (Technica, SMF28-C; FBGS, DTG-LBL). The FBG was attached on the surface of test objects via commercially available superglue (Pattex Ultra Gel).
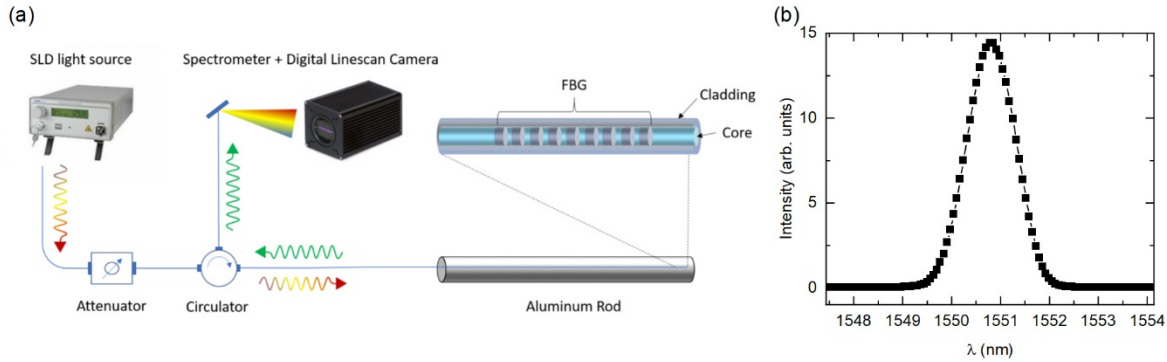


Figure 8: (a) Schematic drawing of the FBG interrogation setup using a broadband superluminescent diode (SLD) as light source and a digital linescan camera to detect the reflection peaks. (b) Reflection peak of a single 3mm long FBG.

### 2.3.1   FBG Resonance Testing

As a proof of principle, we carried out measurements of mechanical resonances on an aluminum rod of diameter d = 2.23 cm, and length l = 165.9 cm. The dimensions of the rod were chosen to shift its mechanical resonances below 5000 Hz due to the limited line rate of the camera. FBG's with a length of 3 mm were chosen for this experiment. The rod was suspended at two points via nylon threads to ensure quasi free boundary conditions. The resonances were excited with a slight hammer tap at the end of the rod.

Fig. 9a shows a snapshot of a typical strain vs. time signal with strain amplitudes up to 10 με. Due to memory limitations of the data acquisition card, we can either record the entire 1024 pixel range for 100 ms or limit the range to 50 pixel and record one reflection peak over a time interval of ≈ 4 s. The resulting Fast Fourier Transforms (FFT's) of the strain signal are shown in Fig. 9b and (c) respectively. Each peak corresponds to a mechanical resonance of the aluminum rod. Note that due to the longer acquisition time window resonances appear much sharper in Fig. 9c. The relative amplitude of the peaks also varies between Fig. 9b and (c), indicating that some resonances experience a larger attenuation than others. Overall, the measured resonance frequencies match well with those calculated with finite element simulations and we can capture a significant portion of the resonances with only a single FBG within a short time frame 100 ms.
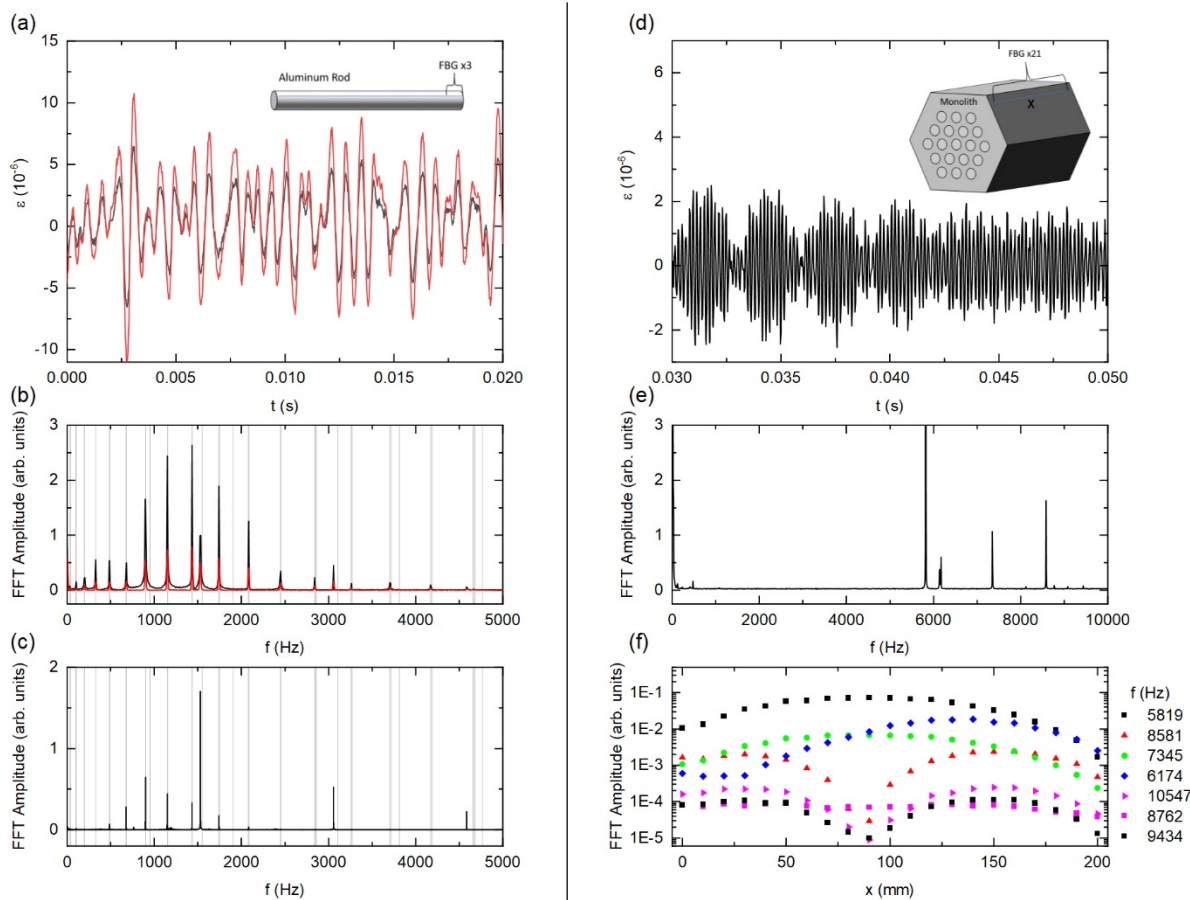
Figure 9: Mechanical resonances observed in an aluminum rod (a-c) and a 3D printed steel monolith as part of a micro reactor assembly (d-f). (a) Strain vs. time measured via two FBG's located close to one end of the aluminum rod. (b) FFT's of the signals shown in (a) collected over a 100 ms time interval. The light gray vertical lines mark the resonance frequencies obtained from finite element simulations. (c) FFT of the strain signal of a single FBG interrogated over a time interval of 4 s. (d) Strain vs. time measurement of a single FBG that is part of an array of 21 gratings attached to the side of the micro reactor monolith as shown in the inset. (e) FFT of the strain signal shown in (d) obtained over a 4 s time interval. (f) FFT amplitude of multiple mechanical resonances as a function of the center position x of each individual grating distributed over the length of the monolith.

Similar measurements were performed on a 3D printed hexagonal steel monolith representing a prototype part of a microreactor. An array of 21, 10 mm long, FBG's were attached to one side of the monolith as depicted in Fig. 9d. Thus, the length of the FBG array almost spans the entire length of the monolith. Mechanical resonances were again excited via a slight hammer tap to the face of the monolith. A typical strain vs. time signal is shown in Fig. 9d. Note the significantly smaller amplitude and larger attenuation of the resonances in the monolith when compared to the aluminum rod - likely related to structural defects due to the 3D printing process. Regardless of the smaller strains, we were able to observe at least seven resonances (Fig. 9e) and were able to track their amplitude over the length of the monolith (Fig. 9f). The resulting strain profiles of the measured resonances are in good agreement with other experiments involving 3D scanning laser vibrometry, this can be seen in Fig. 10.
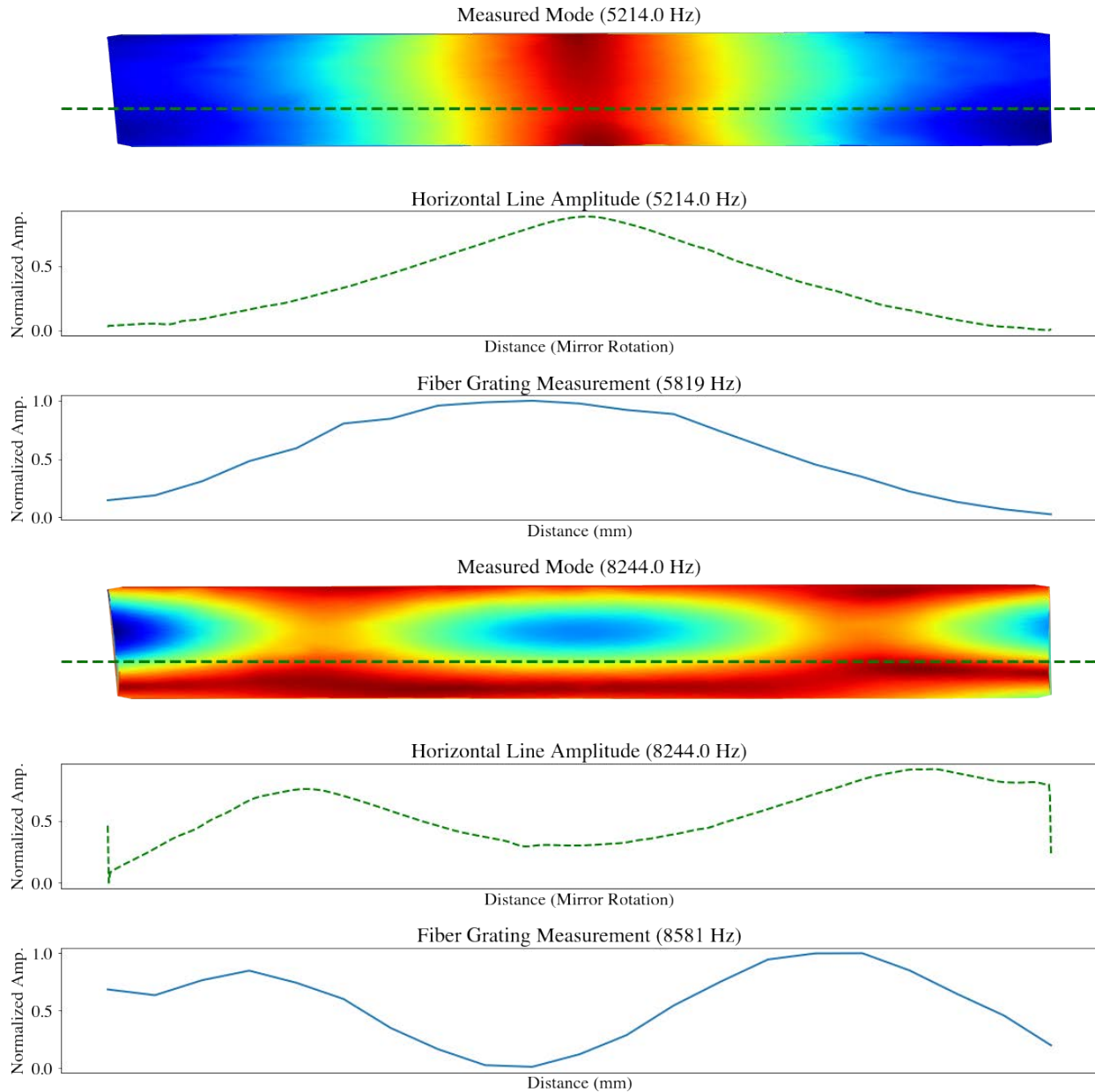
Figure 10: The color image shows a scan made with the 3D scanning laser vibrometer, the green dashed line through the image shows a location where the amplitudes of the scanning grid are extracted for the particular mode shape (this location is selected to align with the placement of the FBG), these amplitudes are plotted in the green dashed line. The blue line is the extracted FBG mode shape. There is good agreement between the FBG and laser vibrometry data.

An attempt was made to excite mechanical resonances in the monolith via a white noise signal coupled into a piezoelectric transducer that was attached to the monolith. The white noise frequency was cut off above 10 kHz to focus the excitation on the frequency region detectable with our current setup. We were able to observe a single resonance at 5819 kHz, which is also the dominant resonance in the spectra obtained from the hammer impact excitation. No further resonances were observed with this technique.

### 2.3.2 Acoustic Emission

Among several technologies that are currently in use for structural health monitoring, the acoustic emission (AE) technique aims to detect stress waves generated by the formation/propagation of fractures in a material. As reported in refs. [8,9], FBG's are a promising avenue for structural health monitoring via measurements of AE events. Furthermore, one can obtain information about the fracture location by simultaneously interrogating of multiple FBG's distributed over the surface of a part/structure, due to the different time of arrival for the associated stress waves that travel at the speed of sound in the material. We tested such a scenario by attaching two FBG sensors to the opposite ends of an aluminum rod (same as above) and tap the rod with a hammer at one end to generate the acoustic wave.

Fig. 11a shows the strain response of two FBG's. A closer look at the beginning of the AE signal (Fig. 11b) reveals that the onsets of the AE signals are separated by $\approx 0.28$ ms or 13 lines (at a line rate of 46992 Hz). Given the sound velocity in aluminum ($\approx 6100$ m/s), this corresponds to a distance of 169 cm between the two gratings - the measured distance is 157 cm. If the AE is generated in the center of the rod, no separation in the onset of the AE signal is detectable (Fig. 11c). As expected, these results reveal the location where the tap is originated with an uncertainty $E_{rr}$ determined by the time interval between spectra and the speed of sound of the material. Indeed, $E_{rr} = 6100$ m/s / 46992 Hz = 13 cm confirming excellent agreement in our experiment. A location resolution 5x better ($\approx 2.5$ cm) can be achieved with a similarly faster interrogation protocol, available in state-of-the-art commercial linescan cameras.
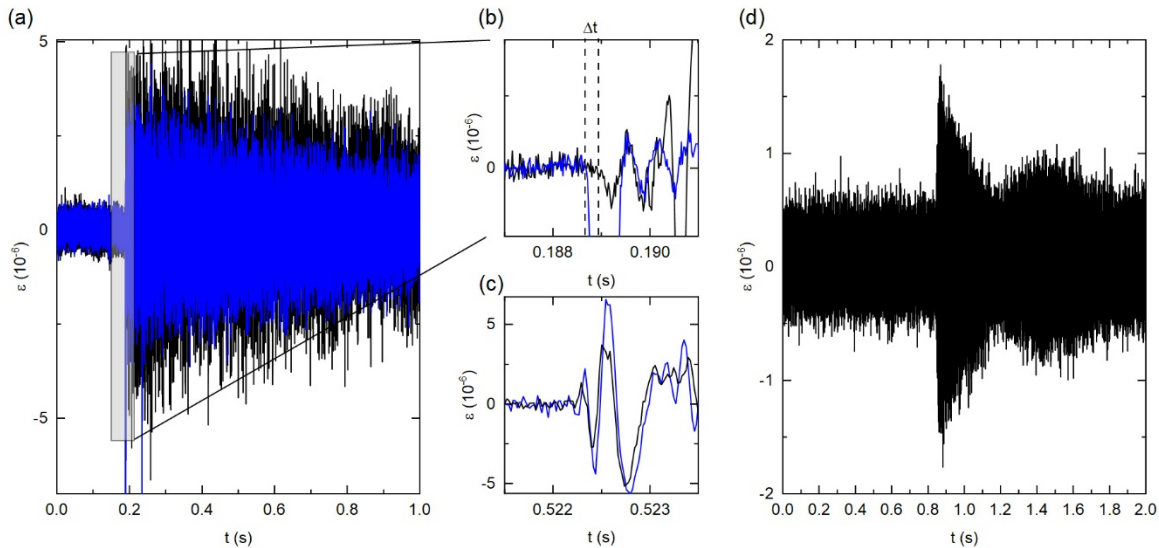


Figure 11: Acoustic emission tests on an aluminum rod. (a) Strain vs. time for two FBG's located 1.57 m apart at the ends of the aluminum rod. The zoomed view (b) shows the onset of the acoustic emission signal which was generated by a slight hammer tap on one end of the rod. (c) Onset of the acoustic emission signal when the rod is tapped in the center. (d) Acoustic emission signal induced by a lead pencil break at the surface of the aluminum rod.

A common technique to generate AE signals is breaking a pencil lead on the surface of the test object. We confirmed that the acoustic wave generated by such a pencil break event can be detected with our FBG measurement technique (Fig. 11d). However, comparison of the AE signals detected by different gratings is still difficult, which makes a quantitative analysis challenging. Overall, a significantly higher interrogation rate is desirable for the AE detection to enable a more precise location of the AE event.

### 2.3.3　Irradiation test

Irradiation tests were performed on polyimide coated radiation resistant pure silica FBG arrays (Technica, T-80) as well as regular $GeO_2$ doped FBG arrays (Technica, SMF28-C) in the Mark 1 irradiation facility at LANL. The FBG's were exposed to an overall dose of $\approx$ 40 kGy over a period of 2127.25 min. No clear systematic Bragg wavelength shift (BWS) $\Delta\lambda$ was observed when comparing the center wavelength of each grating of regular and radiation resistant fibers (Fig. 12a) after accounting for temperature differences.

According to ref. [8], differences in the manufacturing processes have the biggest impact on the performance of FBG in radiation environments with regards to a radiation induced BWS and/ or change in the peak width and peak attenuation. Differences in the $GeO_2$ content or $H_2$ loading before inscription of the gratings are of minor importance. In general, radiation induced BWS of 50-100 pm were observed at a dose of 40 kGy with most FBG's showing signs of saturation at doses up to 100 kGy. As one would expect, with the exception of FBG sensor #4, the RR FBG's tested here show a significantly smaller BWS than the regular fibers. These preliminary results point to the need for longer and more controlled radiation exposures, with on-site monitoring of the fibers that eliminates the need for relocation, bending, and temperature corrections that can effectively mask the small impact of irradiation on the FBG sensors performance.
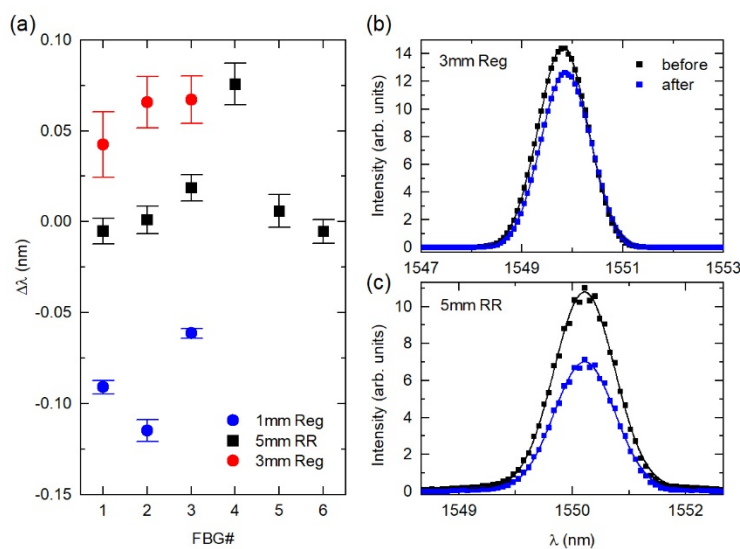


Figure 12: Test measurements on irradiated fibers. (a) Shift in the center wavelength $\Delta\lambda$ of regular (Reg) and radiations resistant (RR) FBG's after irradiation. Note that different FBG sensors (#1-#6, depending on the fiber) placed on different optical fibers 1mm Reg (blue), 3 mm Reg (red), and 5mm RR (black), show different responses to irradiation. (b) Reflection peak of a 3mm regular FBG before (black) and after (blue) irradiation. (c) Reflection peak of a 5mm radiation resistant FBG before (black) and after (blue) irradiation.

## 3　Summary

This report demonstrates the applicability of RUS and NRUS techniques in detecting changes in a material. It also demonstrates that these two techniques can be conducted using passive monitoring of background noise, meaning these techniques lend themselves very well to embedded passive sensing. Coupling the two with FBG sensing improves the technology by providing temporal as well as spatial

data, allowing for all previously developed techniques to be employed seamlessly with FBG. With the ability to also detect acoustic emission, further techniques can be used that are common to seismic applications to locate source emission.  Future work will be necessary to characterize operational and ambient noise to assess the ability to utilize the available noise for the specific components and monitoring applications.

# 4    References

1. Beardslee, Luke B., Marcel C. Remillieux, and T. J. Ulrich. "Determining material properties of components with complex shapes using Resonant Ultrasound Spectroscopy." Applied Acoustics 178 (2021): 108014.

2. TenCate, James A., and Paul A. Johnson. "Nonlinear resonant ultrasound spectroscopy: assessing global damage." Nonlinear Ultrasonic and Vibro-Acoustical Techniques for Nondestructive Evaluation. Springer, Cham, 2019. 89-101.

3. Satori, K., Fukuchi, K., Kurosawa, Y., Hongo, A. & Takeda, N. Polyimide-coated small-diameter optical fiber sensors for embedding in composite laminate structures. in 285 (2001). doi:10.1117/12.435531.

4. Wu, Q., Okabe, Y. & Yu, F. Ultrasonic Structural Health Monitoring Using Fiber Bragg Grating. *Sensors* **18**, 3395 (2018).

5. Zhu, Y., Hu, L., Liu, Z. & Han, M. Ultrasensitive ultrasound detection using an intracavity phase-shifted fiber Bragg grating in a self-injection-locked diode laser. *Opt. Lett.* **44**, 5525 (2019).

6. Willberry, J. O., Papaelias, M. & Franklyn Fernando, G. Structural Health Monitoring Using Fibre Optic Acoustic Emission Sensors. *Sensors* **20**, 6369 (2020).

7. Jaime, M. *et al.* Fiber Bragg Grating Dilatometry in Extreme Magnetic Field and Cryogenic Conditions. *Sensors* **17**, 2572 (2017).

8. Wild, G. & Hinckley, S. Acousto-Ultrasonic Optical Fiber Sensors: Overview and State-of-the-Art. *IEEE Sensors J.* **8**, 1184–1193 (2008).

9. Jinachandran, S. & Rajan, G. Fibre Bragg Grating Based Acoustic Emission Measurement System for Structural Health Monitoring Applications. *Materials* **14**, 897 (2021).

10. Henschel, H., Hoeffgen, S. K., Krebber, K., Kuhnhenn, J. & Weinand, U. Influence of Fiber Composition and Grating Fabrication on the Radiation Sensitivity of Fiber Bragg Gratings. *IEEE Trans. Nucl. Sci.* **55**, 2235–2242 (2008).